Comparison of Approaches for Measuring and Predicting the Viscosity of Ternary Component Aerosol Particles

Grazia Rovelli,[†,∥] Young-Chul Song, [†,⊥] Adrian M. Maclean,[‡] David O. Topping,[§] Allan K. Bertram, [‡] Jonathan P. Reid[†,*]

[†] School of Chemistry, University of Bristol, Bristol, BS8 1TS, UK

[‡] Department of Chemistry, University of British Columbia, Vancouver, BC, V6T 1Z1, Canada

[§] School of Earth, Atmospheric and Environmental Science, University of Manchester, Manchester M13 9PL, UK

ABSTRACT: Measurements of the water activity-dependent viscosity of aerosol particles from two techniques are compared, specifically from the coalescence of two droplets in a Holographic Optical Tweezers (HOT) and poke-and-flow experiments on particles deposited onto a glass substrate. These new data are also compared with the fitting of Dimer Coagulation, Isolation and Coalescence (DCIC) measurements. The aerosol system considered in this work are ternary mixtures of sucrose-citric acid-water and sucrose-$NaNO_3$-water, at varying solute mass ratios. Results from HOT and poke-and-flow are in excellent agreement over their overlapping range of applicability (~10^3-10^7 Pa s); fitted curves from DCIC data show variable agreement with the other two techniques because of the sensitivity of the applied modelling framework to the representation of water content in the particles. Further, two modelling approaches for the predictions of the water activity-dependent viscosity of these ternary systems are evaluated. We show that it is possible to represent their viscosity with relatively simple mixing rules applied to the subcooled viscosity values of each component or to the viscosity of the corresponding binary mixtures.

Viscosity is the physical property that characterizes the resistance of a fluid to deformation. It is the quantity that is measured or inferred to assign the phase state of organic aerosol particles, which can be liquid (viscosity <10^2 Pa s), semi-solid (viscosity between 10^2 and 10^{12} Pa s) or solid (above the glass transition, viscosity higher than 10^{12} Pa s).[1] Indeed, laboratory and field studies have demonstrated that atmospheric organic aerosol (OA) particles can exist in liquid, highly viscous or glassy states, depending on the formation conditions (e.g. semi volatile organic precursor identity [2–4] and concentration[5]) and on the environmental conditions of the surrounding gas phase (temperature, T, and relative humidity, RH). The viscosity of a particle decreases with increasing temperature and with increasing water content (i.e. increasing RH) due to the plasticizing effect of water.[6] The phase state of atmospheric organic aerosol particles affects many of their chemical-physical properties and various processes they are involved in within the atmosphere. Viscous particles are characterized by longer timescales of equilibration to the surrounding gas-phase for the partitioning of both water[7–10] and semivolatile organic components[11–14] between the gas and the condensed phases. In addition, the slow diffusion of the reactants and products of heterogeneous reactions occurring at the surfaces of viscous aerosol particles can influence the rates of such reactions.[15–18] These two factors combined eventually determine the chemical composition of atmospheric organic aerosols, controlling their optical properties, hygroscopicity and surface tension. Furthermore, semi-solid or solid aerosol particles may act effectively as ice condensation nuclei,[19–21] influencing the properties of clouds and precipitations. All of these processes and properties of atmospheric OA can impact on climate, visibility and human health,[4,22–24] which makes the characterisation of the viscosity of aerosol particles crucial to improve our understanding of their impacts.

To measure the viscosity of aerosol particles over so many orders of magnitude (10^{-3} to 10^{12} Pa s), several complementary analytical techniques have been reported in the literature.[1] Different experimental approaches allow access to different viscosity ranges and conditions in the gas phase surrounding the tested aerosol. It is crucial to assess the reproducibility and the consistency of results obtained from measurements based on different chemical-physical observations. In addition, aerosol particles readily exist in metastable supersaturated solute states limiting the applicability of bulk viscosity measurements (i.e. with viscometers) and, thus, requiring direct measurements in the aerosol phase.

The chemical composition of atmospheric aerosols is complex, including thousands of different organic molecules and inorganic components. In order to rationalize the chemical-physical properties and behaviour of such complex atmospheric aerosols, one of the strategies that is currently used in aerosol science is a laboratory-based bottom-up approach.[25] Involving the study of increasingly compositionally-complex aerosol systems, starting from simple binary aerosols (water and one organic or inorganic component) and successively building up in complexity, fundamental insights into the factors governing aerosol particle phase can be assessed and general principles established. Such a regulated approach can resolve key uncertainties in aerosol microphysics and chemistry and can be valuable in assessing the viscosity of aerosol particles and assigning their

phase state.[1,25] For this reason,[26] we apply here such a bottom-up strategy, reporting measurements and predictions of the viscosity of ternary mixtures of water, organic and inorganic components. Specifically, we consider ternary water-sucrose-citric acid and water-sucrose-$NaNO_3$ mixtures, with variable mass ratios of the solutes. Sucrose and citric acid are representative of the highly oxygenated species that are common in atmospheric aerosol and can be considered proxies of OA; sodium nitrate is also found atmospheric aerosols.

In this publication, we have the two aims of comparing different analytical techniques for the measurement of the viscosity of aerosol particles and of characterizing and modelling the viscosity of ternary aqueous mixtures of organic and inorganic components.

Two experimental approaches are used in this work: the coalescence of two droplets within a Holographic Optical Tweezers (HOT)[26–28] and Poke-and-Flow experiments[29,30] on aerosol samples. In addition, the results are compared with recently published data on the viscosity of the same ternary systems obtained with a Dimer Coagulation, Isolation and Coalesce technique (DCIC).[31] These three approaches are ideally suited to measurements over different viscosity ranges; advantages and limitations associated to each of the techniques considered in this work are discussed in the Results and Discussion session. Finally, the DCIC technique[31–33] gives unique information on the temperature dependence of the viscosity of an aerosol system, but can only be used to infer the RH (and temperature) at which the viscosity of the aerosol system is ~$5 \cdot 10^6$ Pa s.

Besides aiming at the comparison of three complementary analytical techniques for the determination of viscosity of aerosol particles, the aerosol systems we report here are ternary mixtures of water, organic and inorganic components. The data for such aerosol systems are particularly limited[28,34,35] and this works represents an interesting opportunity to test some predictive models of viscosity that remain relatively unvalidated against systems with viscosities above 1 Pa s.[1] More specifically, we have applied the ideal Bosse mixing rule [36] and a mole fraction mixing rules of binary viscosity values rather than the subcooled pure component viscosity. In the following section, we review the experimental and modelling methods before presenting comparative measurements of viscosity using the different techniques and an assessment of the models for viscosity prediction.

EXPERIMENTAL METHODS AND PREDICTIVE MODELS

Holographic Optical Tweezers (HOT). The coalescence of two optically trapped solution droplets within an HOT has been used to infer the viscosity of aqueous solution droplets in the range 10^{-3}-10^9 Pa s.[26–28] In the experimental setup used in this work (Figure 1(a)), two optical traps are formed with a continuous wave 532 nm laser (Laser Quantum Opus 3W) using a Spatial Light Modulator (SLM, Hamamatsu X10468), which is conjugated to the back aperture of a high numerical aperture microscope objective (Olympus ACH, 100×/1.25, oil). An aqueous solution of desired chemical composition is nebulized and delivered to the trapping cell, where individual droplets (3 to 10 μm in radius) can be confined within the two optical traps. The relative humidity in the trapping cell is controlled by mixing dry and humidified nitrogen flows at specific ratios, and measured with a capacitance RH probe (Honeywell, HIH-4202A, ±2% uncertainty on RH) placed after the trapping cell. All measurements were conducted at ambient T (295 K).

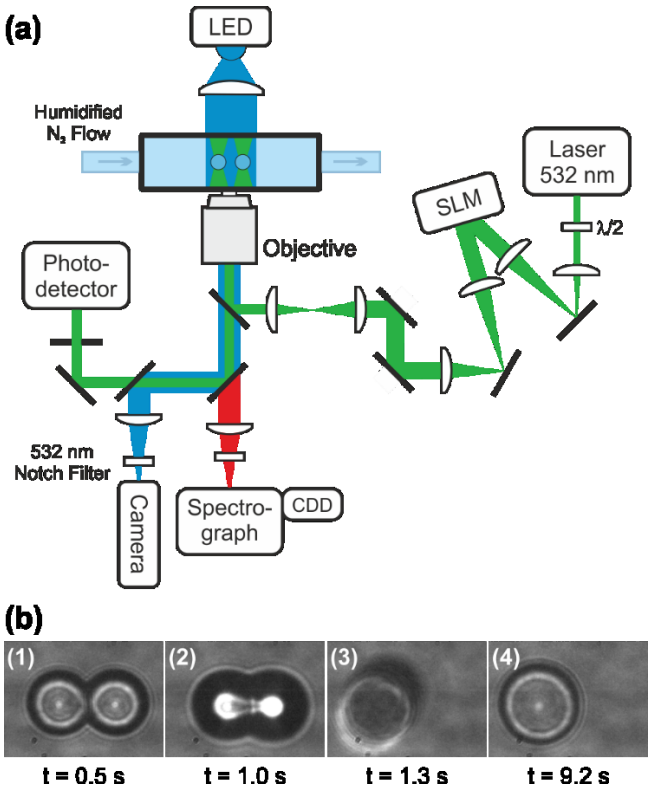

Figure 1. (a) Holographic Optical Tweezer (HOT) experimental setup. (b) Brightfield images of two coalescing droplets (sucrose/critic acid 60/40 wt% mixture, RH=39%). The aspect ratio is inferred for time-points at which the composite non-spherical particle is clearly situated in the image plane.

The inelastically back-scattered light is collected with a Raman spectrograph; the stimulated sharp peaks at wavelengths commensurate with whispering gallery modes in the cavity-enhanced Raman spectra are used to keep track of the size and refractive index of the trapped droplets over time, with an accuracy of ±0.05% for both quantities.[37,38] Prior to coalescence, the two confined droplets are left to equilibrate with the surrounding gas phase. When the particle radius attains a constant value, it is assumed that the droplets have reached an equilibrium moisture content with the gas phase in the trapping cell. The positions of the two optical traps are then modified using the SLM and the two droplets are brought together until they coalesce; the resulting combined particle is kept in the trap until it relaxes to a sphere (Figure 1(b)).

The viscosity can be estimated from the observation of a coalescence event according to previous work[26,28] and as summarized below. For viscosity values lower than a critical value (size-dependent, ~20 mPa s for a droplet radius of 10 μm), two coalesced droplets relax to a sphere through a series of damped oscillations. The amplitude of the oscillation ($A(t)$) is described by Eq. (1):

$$A(t) = \sum_l \exp\left(-\frac{t}{\tau_l}\right) A_{0,l}(cos\omega_l t) \qquad (1)$$

where l indicates the deformation mode of the oscillating coalesced droplet, $A_{0,l}$ is the initial amplitude and ω_l is frequency.

τ_l is the damping timescale, which is dependent on the final droplet size (a), its density (ρ) and viscosity (η):

$$\tau_l = \frac{a^2 \rho}{(l-1)(2l+1)\eta} \quad (2)$$

The damping time is experimentally determined by collecting the elastically scattered light from two coalescing droplets with a photo-detector connected to an oscilloscope. The resulting scattering pattern is fitted with an exponential decay function, as shown in Figure S-1(a), and the viscosity can then be estimated assuming the relaxation is representative of damping in the lowest oscillation mode ($l = 2$) from Eq. (3):

$$\eta = \frac{a^2 \rho}{5\tau} \quad (3)$$

For the measurements in this work, densities of the analysed mixtures were calculated with the ideal mixing rule based on the retrieved value of the particle refractive index.[39] No other assumptions are required and the viscosity can be inferred from the measured characteristic oscillation damping time.

For viscosities higher than the size-dependent critical value mentioned above, the oscillations are overdamped and the two coalesced droplets slowly relax to a single spherical shape. In this case, the amplitude is characterized by a characteristic time given by Eq. (4):

$$\tau_l = \frac{2(l^2+4l+3)}{l(l+2)(2l+1)}\frac{\eta a}{\sigma} \approx \frac{\eta a}{\sigma} \quad (4)$$

where σ is surface tension; damping of high order modes is sufficiently strong that only the $l = 2$ mode must be considered when describing the shape relaxation. Brightfield images of the relaxing particle are collected and the aspect ratio (defined as the ratio between the diameter of the two coalescing droplets along the coalescence axis and the diameter in the perpendicular axis) is calculated from the collected images (Figure S-1(b)). The resulting aspect ratio vs. time data are fitted with an exponential decay function to estimate the relaxation timescale, τ, and the viscosity according to Eq. (3). The uncertainty associated with the fit of the damping time is typically of ±5%.[26] For simplicity, in all the estimations of viscosity presented here, the particle was assumed to have a surface tension equal to that of pure water (72.8 mN m^{-1} at 293 K). Song et al.[26] reported that the uncertainty introduced by such approximation is much smaller than the uncertainties associated with the damping time.

Poke-and-flow. By coupling poke-and-flow experiments and fluid dynamics simulations, it has been possible to measure the viscosity of both aqueous solutions droplets[29,30] and of laboratory SOA particles.[4,5,18,23,40] In such experiments, droplets deposited onto a glass substrate are poked with a sharp needle. The timescale for relaxation in shape from a non-equilibrium half-torus geometry to an equilibrium spherical cap morphology is then observed.

The poke-and-flow setup used in this work is shown in Figure 2(a). Droplets of the tested solution (50-100 µm in diameter) are nebulized onto a glass coverslip with a hydrophobic coating. The coverslip is then mounted on a flow cell coupled to a microscope (Zeiss Axiom Observer) and humidified nitrogen is passed through the cell (flow rate of ~1200 sccm). The relative humidity within the cell is monitored by means of a dew-point hygrometer (General Eastern) placed after the flow cell, whereas the temperature is measured with a thermocouple placed just below it. Calibration of the hygrometer is achieved by measuring the deliquescence relative humidity (DRH) of $(NH_4)SO_4$ and K_2CO_3 and comparing the measured DRH-values with reference values (80.3% and 43.2% RH at 20°C for the two salts, respectively).

Before poking, droplets are left to equilibrate with the surrounding gas phase for at least two hours. Figure S-2 examines the sensitivity of the estimated viscosity on the equilibration time for a range of RH-values (10.2 % to 32.6 % RH) and for a 60/40 sucrose/citric acid wt% mixture. An inferred viscosity increasing with equilibration timescale would indicate that insufficient time was allowed for the droplets to become equilibrated with the surrounding gas phase. However, no systematic dependence is observed for times ≥ 2 hours. No effect of particle size on the retrieved viscosities is observed (Figure S-2). The same conclusion also applies to experiments with other compositional ratios, with the viscosity range the same for all the samples. For both HOT and poke-and-flow, viscosity measurements are conducted at equilibrium and therefore RH and a_w are interchangeably used throughout this paper.

After equilibration, the deposited solution droplets are poked with a needle mounted on a micromanipulator (Nairnshire, MO-202U), with translation of the needle in three dimensions. Tungsten needles with 1 µm tips were used; needles were coated with a hydrophobic coating (Dursan from Silcotek) for high viscosity samples, to prevent the particles sticking to the needle. Images of the poked particles relaxing from a non-equilibrium half-torus geometry to a spherical cap morphology are collected with a CCD camera (Figure 2(b)).

In order to retrieve the upper and lower limits of viscosity of a poked particle, a fluid dynamics simulation (COMSOL Multiphysics) is used according to the work of Renbaum-Wolff et al.[40] and Grayson et al.[30] Briefly, the Navier-Stokes equation is applied for the description of the transport of mass and momentum within the fluid and the Lagrangian-Eulerian method is used to follow the evolution towards a spherical cap geometry, which minimises the surface energy of the modelled system. The parameters needed in the fluid dynamics simulation are contact angle, solution density, surface tension and slip length. All the parameters used for the fluid dynamics simulations in this work are summarized in Tables S-1 and S-2.

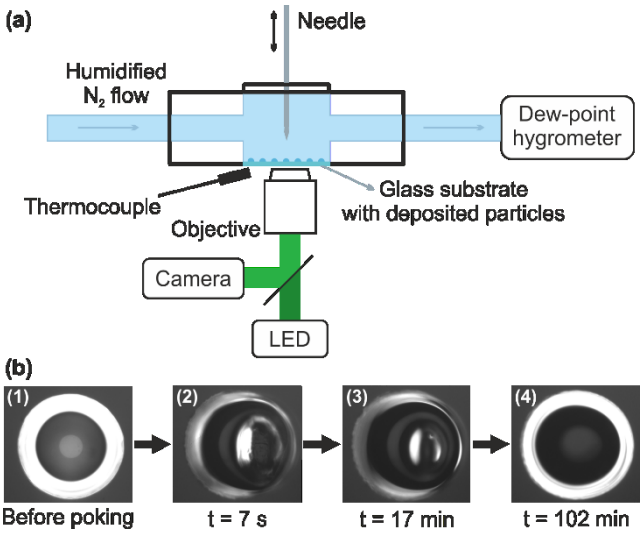

Figure 2. (a) Poke-and-flow experimental setup. (b) Images of an 80/20wt% sucrose/citric acid particle before (1) and after poking (2) – (4). Time after poking is indicated below the images in (2)-(4).

The uncertainties in the viscosity inferred from coupling poke-and-flow experiments with fluid simulations have been extensively discussed by Grayson et al.[30] The uncertainty on the upper and lower limits of viscosity reported in the figures in the Results and Discussion section represent the standard deviation of multiple measurements carried out at the same RH. All the measurements were taken at room temperature (292-293 K).

VFT fit of Dimer Coagulation, Isolation and Coalesce (DCIC) data. We report here in this work new measurements of viscosity using the optical tweezers and poke-and-flow methods and compare them with previously reported values obtained with the DCIC technique.[31–33] To provide a comprehensive comparison here, we present a summary of the DCIC approach for measuring and reporting viscosity values.

In DCIC experiments, two stream of size-selected particles of opposite charges are brought together in a coagulation chamber, where a ramp in either temperature or RH is performed.[31–33] The degree of sintering of dimers formed by the coalescence of two particles with opposite charge is dependent on the viscosity of the particles themselves and, using a modified sintering theory,[41] the T and RH at which the viscosity of the aerosol system is $5 \cdot 10^6$ Pa s can be inferred. By applying the model framework presented in previous publications and described below, the phase state diagrams of the studied aerosol system can be obtained and the water activity-dependent viscosity can be also modelled. The Gordon-Taylor mixing rule[42] is employed to compute the glass transition temperature of the ternary mixture ($T_g(a_w)$, eq. (5)). We use the rearranged equation and the fitted Gordon-Taylor parameters (k_i) from Marsh at al.[31]

$$T_g(a_w) = \frac{(1-w_s)T_{g,w} + w_s \sum_i k_i \varepsilon_i T_{g,i}}{1 - w_s(1 - \sum_i k_i \varepsilon_i)} \qquad (5)$$

The pure component glass transition temperature values used in this calculation are 220 K for $NaNO_3$,[31] 286 K for citric acid[31] and 341 K for sucrose.[33] Gallo et al.[44] summarise the controversy around the value of the glass transition temperature of water ($T_{g,w}$); following the discussion in their work, $T_{g,w}$ was set at 136 K. The mass fractions of solute (w_s) for the binary solutions of sucrose, citric acid and sodium nitrate are represented with a mass-based hygroscopicity parameter κ_m (eq. (6), parameterisations from the supplement of ref. [31]). To represent the hygroscopicity of the ternary mixtures in this work, a mass fraction (ε_i) mixing rule is applied to the binary κ_m values on the entire water activity (a_w) range (eq.(7)).

$$w_s = (1 + \kappa_m(a_w/(1-a_w)))^{-1} \qquad (6)$$

$$\kappa_m(a_w) = \sum_i \varepsilon_i \kappa_{m,i}(a_w) \qquad (7)$$

For comparison with the HOT and poke-and-flow water activity-dependent viscosity measurements, the Vogel-Fulcher-Tamman equation (VFT, eq.(8)) is used to calculate the dependence of viscosity on water activity at the fixed temperature of 295 K:[42]

$$log_{10}(295\ K, a_w) = A + \frac{B}{295 - (T_0 - \Delta T_g(a_w))} \qquad (8)$$

A, B and T_0 are literature fitted parameters[31] and $\Delta T_g(a_w) = T_{g,s} - T_g(a_w)$, where $T_{g,s}$ is the glass transition temperature at $a_w = 0$ ($w_s = 1$ in eq.(5)).

Modelling the viscosity of ternary aerosols. Two different approaches are applied to predict the water activity-dependent viscosities of ternary aerosols. First, the Bosse mixing rule is evaluated.[36] In previous work, we reported that this approach is the most adequate to represent the viscosity of a series of binary solutions of saccharides, carboxylic acids and alchools.[26] To estimate the viscosity of a mixture (η_{mix}), the subcooled pure component viscosities of each component ($\eta_{i,sub}$) are needed according to Eq. (9):

$$\ln(\eta_{mix}) = \sum_i x_i \ln(\eta_{i,sub}) \qquad (9)$$

where x_i is the mole fraction of the i-component. $\eta_{i,sub}$ values used here come from previous work.[26,45]

We also tested another simple approach to predict the viscosity of ternary aerosols that relies on knowledge of the water activity-dependent viscosities of the corresponding binary mixtures, rather than on the subcooled pure component viscosities as in the Bosse mixing rule. In this approach, the total water content for a mixture at a specific water activity is calculated using equations (6) and (7). It is assumed that the total mass of water in the system (m_{H_2O}) is ideally distributed between the two solutes (1 and 2) according to their relative mass fraction (ε_i), using a Zadanoskii-Stokes-Robinson approach (ZSR,[46] eq. **Error! Reference source not found.**).

$$m_{H_2O} = m_{H_2O,1} + m_{H_2O,2} = \varepsilon_1 \cdot m_{H_2O} + \varepsilon_2 \cdot m_{H_2O} \qquad (10)$$

A "partial" mass fraction for each solute in a hypothetical binary mixture containing a mass of water $m_{H_2O,i}$ is calculated. The corresponding water activity can be obtained from eq. (6) for the binary solution and the "partial" viscosity ($\eta_i(a_w)$) for each solute component calculated. The overall viscosity of the ternary mixture is then calculated with the Arrhenius mixing rule:[47]

$$\ln(\eta_{mix}(a_w)) = \sum_i x_i \ln(\eta_i(a_w)) \qquad (11)$$

where x_i is the mole fraction of the solute i in the mixture at the water activity a_w.

RESULTS AND DISCUSSION

Comparison of experimental techniques. The relative humidity dependent-viscosity for three sucrose/citric acid mixtures (wt% ratios of 80/20, 60/40 and 40/60) measured with poke-and-flow (shaded areas) and HOT (circles) are reported in Figure 3. The HOT measured viscosity for binary citric acid[26] and sucrose[26,28] are also shown for comparison. The agreement between the two experimental techniques used in this work is very satisfactory over their overlapping range of application (~10^3-10^7 Pa s) for all the three sucrose-to-citric acid ratios considered. The combined data obtained with HOT and poke-and-flow experiments is fitted with a second order polynomial (dashes lines, see fitted parameters in Table S-3 and S-4 in the Supporting Information).

Interestingly, neither of the techniques has sufficient accuracy to fully discriminate between the viscosity of the 60/40 and 40/60 sucrose/citric acid mixtures (panels b and c in Figure 3, see also Figure S-3 for a direct comparison of the datasets). Typically, uncertainties associated with both measurements span over ~1 order of magnitude. Indeed, the predicted curves for these two sucrose/citric acid ratios are also found to be close (panels e and f in Figure 3, discussion in the next Section), falling within one order of magnitude. Similar considerations apply when considering the comparison between the HOT and poke-and-flow data for two sucrose/$NaNO_3$ mixtures (wt% ratios of 80/20 and 60/40, Figure 4, panels a and b). The agreement between the datasets obtained with the two different analytical techniques is excellent. This provides further validation of the HOT and poke-and-flow approaches, that are charactercised by complementary experimental capabilities. in facts, the coalescence of two droplets within a HOT allows measurements over a wide range of viscosity (from 10^{-3} to 10^{9} Pa s)[26–28] but requires a relatively large amount of sample solution for nebulization (of the order of mL), making it unsuitable to assess the viscosity of secondary OA (SOA) samples from laboratory chambers. On the other hand, Poke-and-flow experiments can access a more limited range in viscosities (10^{3}- 10^{7} Pa s) but are suitable for measurements on smaller samples of material (e.g. for chamber SOA).[4,5,18,23,40] Figure 5 shows the VFT fits of the DCIC data from Marsh et al.[31] (dotted lines) compared with the polynomial fits of HOT and poke-and-flow data for three sucrose/citric acid mixtures (panel (a)) and two sucrose/$NaNO_3$ mixtures (panel (b)). In the high RH (low viscosity) region, the VFT fit is not able to capture the decrease in viscosity due to the plasticising effect of water. According to Rothfuss and Petters,[33] this is a consequence of the constrained VFT fit through viscosity values around $5 \cdot 10^{6}$ Pa s and the viscosity at the glass transition temperature (10^{12} Pa s). Therefore, the authors indicate 10^{4} Pa s as the lower limit in viscosity that can be represented with this approach. For this reason, the VFT curves in Figure 3 and 4 are not shown below this threshold.

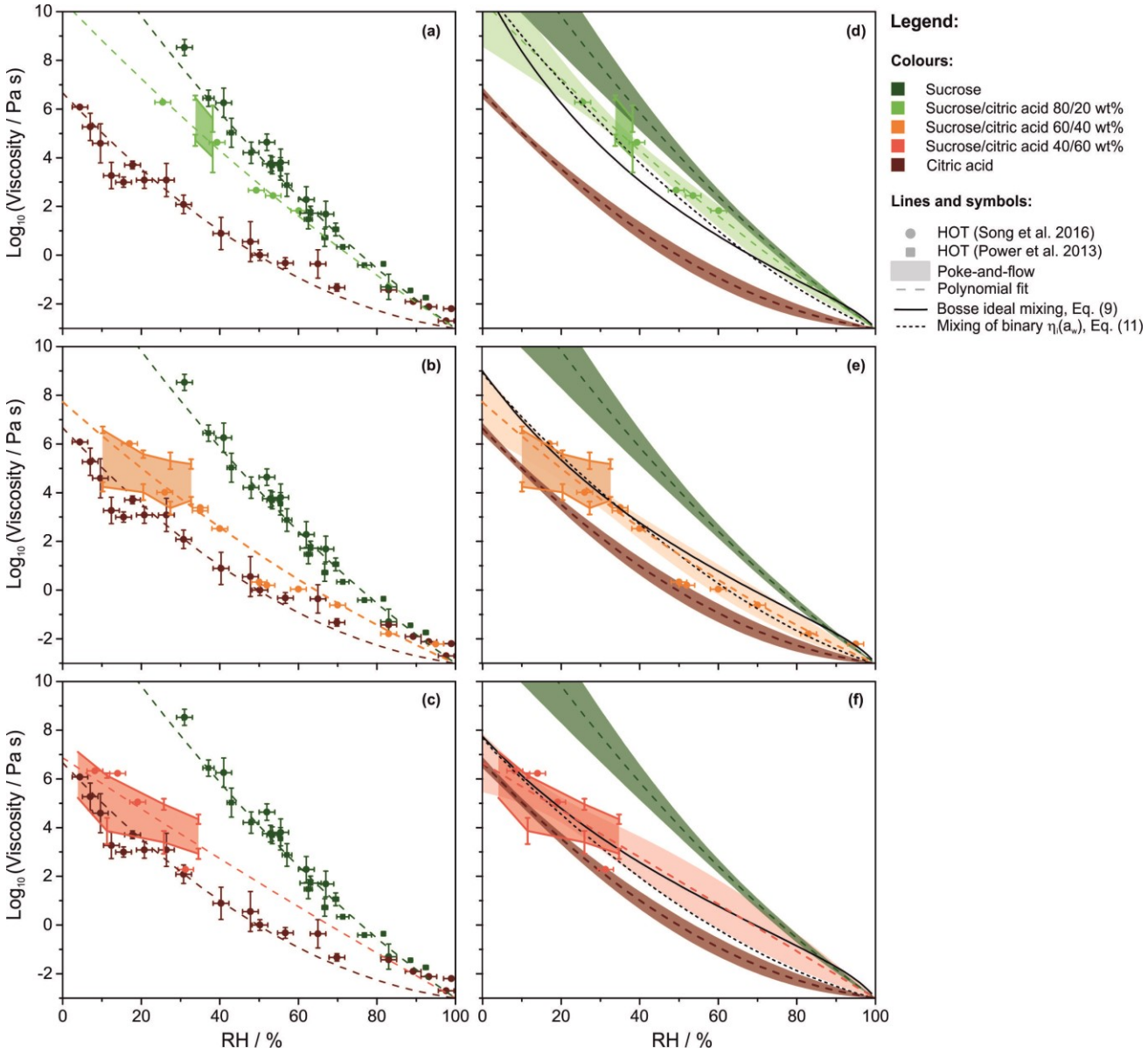

Figure 3. Measured and modelled relative humidity-dependent viscosity of sucrose/citric acid mixtures (80/20 wt%, panels a-d; 60/40 wt%, panels b-e; 40/60 wt%, panels c-f). Data for binary sucrose[26,28] and citric acid[26] are also reported for comparison. Symbols: circles – HOT data (60/40 wt% mixture in panels b and e from previous work);[31] solid lines – poke-and-flow measured upper and lower limits of viscosity (shaded area included to guide the eye); dashed lines – 2nd order polynomial fit of HOT and poke-and-flow data (the envelopes in panels d, e and f represent the 95% confidence bands of the fitting);[31] solid line – prediction from Bosse ideal mixing (Eq. (9)); short dashed line – prediction from mixing of binary viscosity values (Eq. (11)). Colors: dark green – sucrose; light green – 80/20 wt% sucrose/citric acid mixture; orange – 60/40 wt% mixture; red – 40/60 wt% mixture; brown – citric acid.

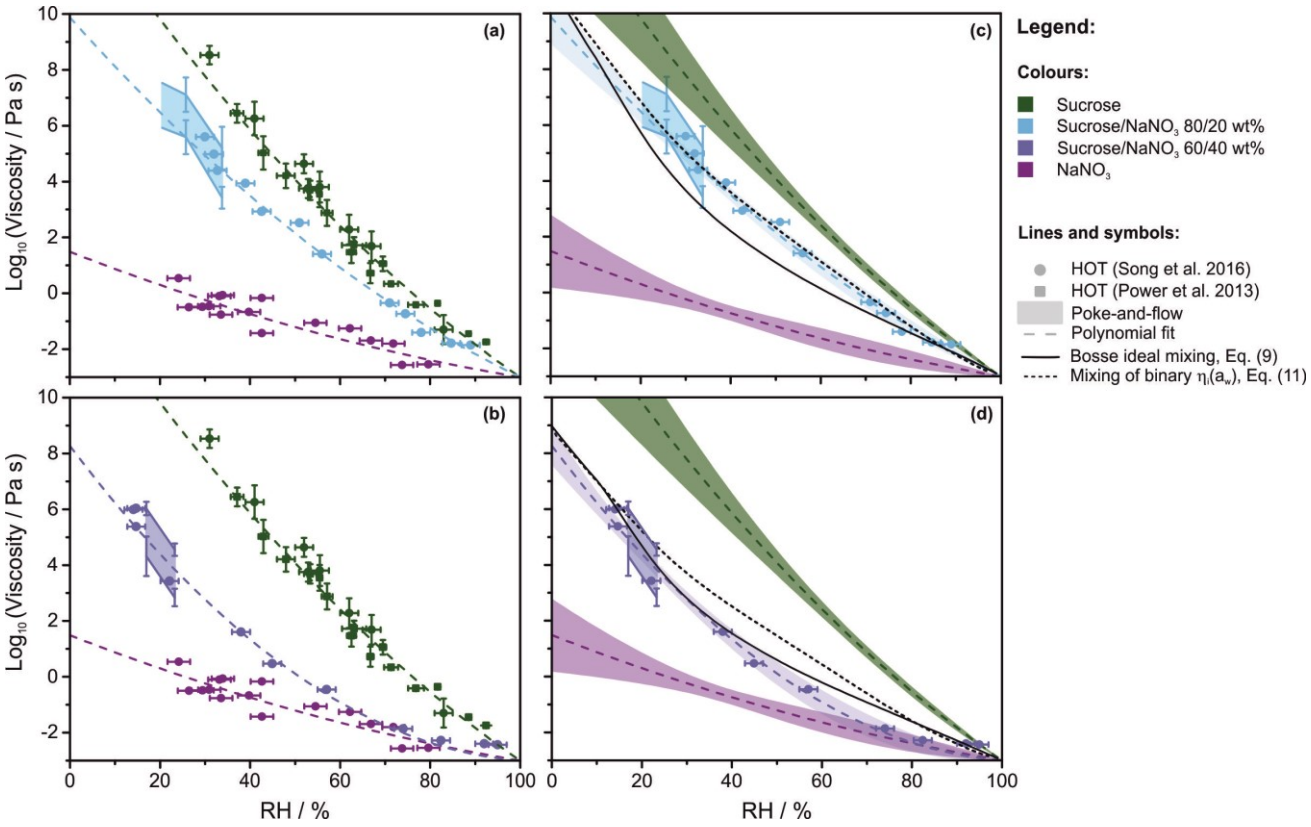

Figure 4. Measured and modelled relative humidity-dependent viscosity of sucrose/$NaNO_3$ mixtures (80/20 wt%, panels a-c; 60/40 wt%, panels b-d). Data for binary sucrose[26,28] and $NaNO_3$[45] are also reported for comparison. Symbols: circles – HOT data; solid lines – poke-and-flow measured upper and lower limits of viscosity (shaded area included to guide the eye); dashed lines – 2nd order polynomial fit of HOT and poke-and-flow data (the envelopes in panels d, e and f represent the 95% confidence bands of the fitting); solid line – prediction from Bosse ideal mixing (Eq. (9)); short dashed line – prediction from mixing of binary viscosity values (Eq. (11)). Colors: dark green – sucrose; light blue – 80/20 wt% sucrose/$NaNO_3$ mixture; indigo – 60/40 wt% mixture; purple – $NaNO_3$.

A comparison between the HOT and poke-and-flow datasets and the VFT curves calculated from the DCIC measurements by Marsh et al.[31] shows good agreement for sucrose[33] the 80/20 sucrose/citric acid mixture (Figure 5, panel (a)) but a lower accord for the 60/40 and the 40/60 mixtures (panel (a)) and for the two sucrose/$NaNO_3$ mixtures (panel (b)). Potential explanations of this disagreement could be found in the representation of the water content in these mixtures in the VFT modelling framework (equations (6) and (7)), which is very sensitive to the input hygroscopicity (see for example Figure 7c in Rothfuss and Petters[33]). The VFT curves tend to overpredict the viscosity of mixtures (even in the range of applicability of the modelling framework, above 10^4 Pa s). A slight underprediction of the hygroscopic properties of complex mixtures would result in an underestimation of the water content and of its plasticising effect. Despite these limitations, the DCIC measurements represent one of the very few techniques in current aerosol science that allows the investigation of the temperature dependence of viscosity of aerosol particles of sub-micrometre size and their glass transition temperature,[1] both of which are crucial to improve our understanding of the ability of atmospheric aerosols to act as ice nuclei.

Modelling the water activity-dependent viscosity of ternary aerosol particles. Song et al.[26] reported that the Bosse mixing rule[36] was best able to predict the viscosity of binary mixtures of a number of organic components.

In this work we applied the ideal Bosse mixing rule[36] (Eq. (9)) together with a mixing of the binary viscosities (Eq. (11)) for the prediction of the viscosities of sucrose-citric acid-water and sucrose-$NaNO_3$-water ternary aerosols (Figure 3 and 4, panels d, e and f). The overall aim is to evaluate the performance of relatively simple mixing rules at representing the water activity-dependent viscosity of increasingly compositionally complex aerosol systems, building upon the work of Song et al.,[26] who indicated the Bosse mixing rule as the most promising in representing the viscosity of binary mixtures of saccharides, alcohols, carboxylic acids. Here, we evaluate its performance in predicting the viscosity of ternary aerosol systems, It should be noted that all of these modelling tools rely on an accurate estimation of the water content at varying relative humidity; for all the predictions in this section, the hygroscopicity of the ternary mixtures is represented according to equations (6) and (7).

The ability of the two modelling approaches to capture the water-activity dependent viscosities is very satisfactory for most of the considered ternary systems. The largest deviation is observed for the 60/40 wt% sucrose/$NaNO_3$ mixture (up to ~1.5 orders of magnitude around RH=50%, Figure 4(d)). The reason of this discrepancy could be that the hygroscopic properties of a mixture containing an highly oxygenated compound and inorganic charged species are likely to be complex and far from ideal (as represented by equations (6) and (7)), and this inaccuracy in the representation of hygroscopicity reflects in an inaccuracy in the resulting viscosity.

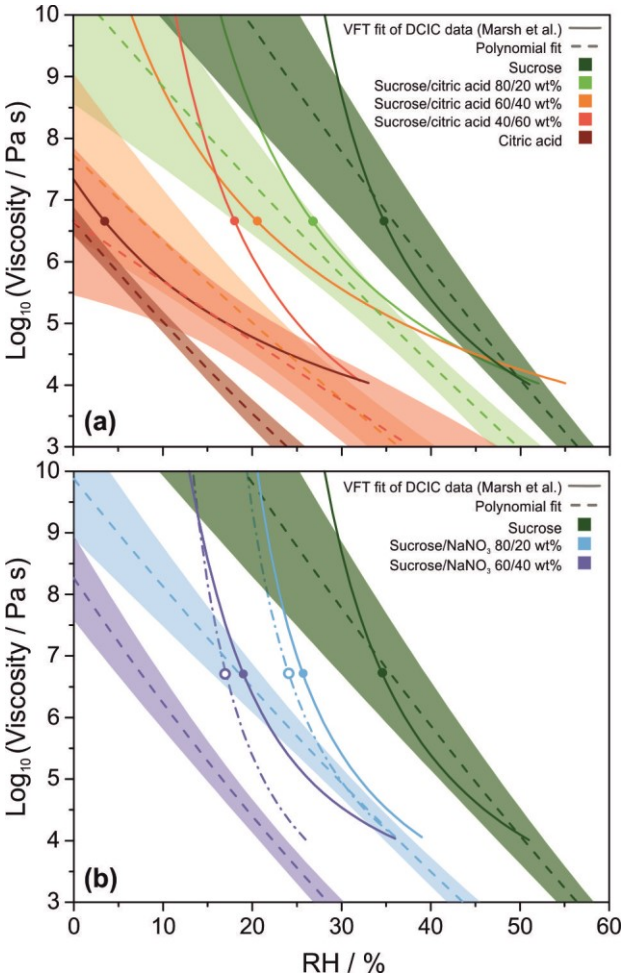

Figure 5. Comparison of polynomial fits of poke-and-flow and HOT measurements (dashed lines, envelopes represent the 95% confidence band of the fitting) and VFT fit of data from Marsh et al.[31] (solid lines) for sucrose/citric acid (a) and sucrose/$NaNO_3$ (b) mixtures. The circles indicate the value of viscosity of $5 \cdot 10^6$ Pa s, at which the DCIC measurements are taken.

In general, it appears that the mixing of the viscosities of the binary solutions (Eq. (11)) is more accurate in representing the viscosity of ternary aerosol systems for all systems excluding the 60/40 wt% sucrose/$NaNO_3$ mixture (Figure 4(d)). It seems likely that mixing the water activity-dependent viscosity of the binary solutions (when data are available) partly encompasses the non-ideality of these ternary mixtures and better represents their viscosity. However, the number of mixtures evaluated in this work is limited and a larger number of measurements would be needed to draw more general conclusions.

CONCLUSIONS

A deeper understanding of the viscosity of aerosol particles would provide a better representation of their phase state in the atmosphere and of their effects on climate and human health.[1] The viscosity of atmospheric aerosol particles spans many orders of magnitudes (10^{-3} to 10^{12} Pa s) and, for this reason, a number of different analytical techniques has been developed in recent years, each characterised by definite ranges of application in viscosity, RH and temperature. Assessing the agreement of these techniques is fundamental to demonstrate they can be complementarily and reliably used to cover different ranges of application.

In this work we have compared poke-and-flow experiments on particles deposited on a coverslip with results from the coalescence of two droplets in a holographic optical tweezers. Excellent quantitative agreement between the two is observed, with measurements consistent within ~1 order of magnitude, the accuracies of the two techniques. In addition, fitted water activity dependent-viscosities from DCIC measurements were also considered and a variable level of agreement with the results from the two other techniques was observed. These discrepancies are likely due to uncertainties in the representation of the hygroscopicity of ternary mixtures within the modelling framework applied to the DCIC data.

Finally, the Bosse ideal mixing rule and the mixing of the binary water activity-dependent viscosities were used to predict the ternary aerosol systems considered in this work. Results from both approaches are in good agreement with the measurements in this work, with the mixing of the binary viscosities appearing to be the most accurate.

ASSOCIATED CONTENT

Supporting Information

The Supporting Information is available free of charge on the ACS Publications website.
The Supporting Information includes three additional figures and four additional tables as indicated in the main manuscript (PDF).

AUTHOR INFORMATION

Corresponding Author

Jonathan P. Reid. E-mail: J.P.Reid@bristol.ac.uk

Present Addresses

‖ Chemical Science Division, Lawrence Berkeley National Laboratory, Berkeley, California 94611, United States.

⊥ Department of Chemistry, Inha University, Incheon, 22212, South Korea

Notes

The authors declare no competing financial interest.

ACKNOWLEDGMENT

G.R., Y.S., D.O.T. and J.P.R. gratefully acknowledge support from NERC through the award of grants NE/N013700/1 and NE/M004600/1. A.K.B and A.M.M. acknowledge support from the Natural Sciences and Engineering Research Council of Canada.

REFERENCES

(1) Reid, J. P.; Bertram, A. K.; Topping, D. O.; Laskin, A.; Martin, S. T.; Petters, M. D.; Pope, F. D.; Rovelli, G. The Viscosity of Atmospherically Relevant Organic Particles. *Nat. Commun.* **2018**, *9*, 956.

(2) Saukko, E.; Lambe, A. T.; Massoli, P.; Koop, T.; Wright, J. P.; Croasdale, D. R.; Pedernera, D. A.; Onasch, T. B.; Laaksonen, A.; Davidovits, P.; et al. Humidity-Dependent Phase State of SOA Particles from Biogenic and Anthropogenic Precursors. *Atmos. Chem. Phys.* **2012**, *12* (16), 7517–7529.

(3) Bateman, A. P.; Bertram, A. K.; Martin, S. T. Hygroscopic Influence on the Semisolid-to-Liquid Transition of Secondary Organic Materials. *J. Phys. Chem. A* **2015**, *119* (19), 4386–4395.

(4) Song, M.; Liu, P. F.; Hanna, S. J.; Zaveri, R. A.; Potter, K.; You,

Y.; Martin, S. T.; Bertram, A. K. Relative Humidity-Dependent Viscosity of Secondary Organic Material from Toluene Photo-Oxidation and Possible Implications for Organic Particulate Matter over Megacities. *Atmos. Chem. Phys.* **2016**, *16* (14), 8817–8830.

(5) Grayson, J. W.; Zhang, Y.; Mutzel, A.; Renbaum-Wolff, L.; Böge, O.; Kamal, S.; Herrmann, H.; Martin, S. T.; Bertram, A. K. Effect of Varying Experimental Conditions on the Viscosity of α-Pinene Derived Secondary Organic Material. *Atmos. Chem. Phys.* **2016**, *16* (10), 6027–6040.

(6) Koop, T.; Bookhold, J.; Shiraiwa, M.; Pöschl, U. Glass Transition and Phase State of Organic Compounds: Dependency on Molecular Properties and Implications for Secondary Organic Aerosols in the Atmosphere. *Phys. Chem. Chem. Phys.* **2011**, *13* (43), 19238.

(7) Price, H. C.; Murray, B. J.; Mattsson, J.; O'Sullivan, D.; Wilson, T. W.; Baustian, K. J.; Benning, L. G. Quantifying Water Diffusion in High-Viscosity and Glassy Aqueous Solutions Using a Raman Isotope Tracer Method. *Atmos. Chem. Phys.* **2014**, *14* (8), 3817–3830.

(8) Wang, B.; O'Brien, R. E.; Kelly, S. T.; Shilling, J. E.; Moffet, R. C.; Gilles, M. K.; Laskin, A. Reactivity of Liquid and Semisolid Secondary Organic Carbon with Chloride and Nitrate in Atmospheric Aerosols. *J. Phys. Chem. A* **2015**, *119* (19), 4498–4508.

(9) Lu, J. W.; Rickards, A. M. J.; Walker, J. S.; Knox, K. J.; Miles, R. E. H.; Reid, J. P.; Signorell, R. Timescales of Water Transport in Viscous Aerosol: Measurements on Sub-Micron Particles and Dependence on Conditioning History. *Phys. Chem. Chem. Phys.* **2014**, *16* (21), 9819–9830.

(10) Price, H. C.; Mattsson, J.; Zhang, Y.; Bertram, A. K.; Davies, J. F.; Grayson, J. W.; Martin, S. T.; O'Sullivan, D.; Reid, J. P.; Rickards, A. M. J.; et al. Water Diffusion in Atmospherically Relevant α-Pinene Secondary Organic Material. *Chem. Sci.* **2015**, *6*, 4876–4883.

(11) Vaden, T. D.; Imre, D.; Beránek, J.; Shrivastava, M.; Zelenyuk, A. Evaporation Kinetics and Phase of Laboratory and Ambient Secondary Organic Aerosol. *Proc. Natl. Acad. Sci. U. S. A.* **2011**, *108* (6), 2190–2195.

(12) Wilson, J.; Imre, D.; Beránek, J.; Shrivastava, M.; Zelenyuk, A. Evaporation Kinetics of Laboratory-Generated Secondary Organic Aerosols at Elevated Relative Humidity. *Environ. Sci. Technol.* **2015**, *49* (1), 243–249.

(13) Yli-Juuti, T.; Pajunoja, A.; Tikkanen, O.-P.; Buchholz, A.; Faiola, C.; Väisänen, O.; Hao, L.; Kari, E.; Peräkylä, O.; Garmash, O.; et al. Factors Controlling the Evaporation of Secondary Organic Aerosol from α-Pinene Ozonolysis. *Geophys. Res. Lett.* **2017**, *44(5)*, 2562–2570.

(14) Zelenyuk, A.; Imre, D. G.; Wilson, J.; Bell, D. M.; Alexander, M. L.; Kramer, A. L.; Massey, S. L. The Effect of Gas-Phase Polycyclic Aromatic Hydrocarbons on the Formation and Properties of Biogenic Secondary Organic Aerosol Particles. *Faraday Discuss.* **2017**, *200*, 143–164.

(15) Hosny, N. A.; Fitzgerald, C.; Vyšniauskas, A.; Athanasiadis, A.; Berkemeier, T.; Uygur, N.; Pöschl, U.; Shiraiwa, M.; Kalberer, M.; Pope, F. D.; et al. Direct Imaging of Changes in Aerosol Particle Viscosity upon Hydration and Chemical Aging. *Chem. Sci.* **2016**, *7* (2), 1357–1367.

(16) Athanasiadis, T.; Fitzgerald, C.; Davidson, N.; Giorio, C.; Botchway, S. W.; Ward, A. D.; Kalberer, M.; Pope, F. D.; Kuimova, M. K. Dynamic Viscosity Mapping of the Oxidation of Squalene Aerosol Particles. *Phys. Chem. Chem. Phys.* **2016**, *18*, 30385–30393.

(17) Shiraiwa, M.; Ammann, M.; Koop, T.; Pöschl, U. Gas Uptake and Chemical Aging of Semisolid Organic Aerosol Particles. *Proc. Natl. Acad. Sci. U. S. A.* **2011**, *108* (27), 11003–11008.

(18) Hinks, M. L.; Brady, M. V.; Lignell, H.; Song, M.; Grayson, J. W.; Bertram, A. K.; Lin, P.; Laskin, A.; Laskin, J.; Nizkorodov, S. A. Effect of Viscosity on Photodegradation Rates in Complex Secondary Organic Aerosol Materials. *Phys. Chem. Chem. Phys.* **2016**, *18* (13), 8785–8793.

(19) Baustian, K. J.; Wise, M. E.; Jensen, E. J.; Schill, G. P.; Freedman, M. A.; Tolbert, M. A. State Transformations and Ice Nucleation in Amorphous (Semi-)Solid Organic Aerosol. *Atmos. Chem. Phys.* **2013**, *13* (11), 5615–5628.

(20) Lienhard, D. M.; Huisman, A. J.; Krieger, U. K.; Rudich, Y.; Marcolli, C.; Luo, B. P.; Bones, D. L.; Reid, J. P.; Lambe, A. T.; Canagaratna, M. R.; et al. Viscous Organic Aerosol Particles in the Upper Troposphere: Diffusivity-Controlled Water Uptake and Ice Nucleation? *Atmos. Chem. Phys.* **2015**, *15* (23), 13599–13613.

(21) Knopf, D. A.; Alpert, P.; Wang, B. The Role of Organic Aerosol in Atmospheric Ice Nucleation – A Review. *ACS Earth Sp. Chem.* **2018**, *2(3)*, 168–202.

(22) Shrivastava, M.; Cappa, C. D.; Fan, J.; Goldstein, A. H.; Guenther, A. B.; Jimenez, J. L.; Kuang, C.; Laskin, A.; Martin, S. T.; Ng, N. L.; et al. Recent Advances in Understanding Secondary Organic Aerosol: Implications for Global Climate Forcing. *Rev. Geophys.* **2017**, *55* (2), 509–559.

(23) Song, M.; Liu, P. F.; Hanna, S. J.; Li, Y. J.; Martin, S. T.; Bertram, A. K. Relative Humidity-Dependent Viscosities of Isoprene-Derived Secondary Organic Material and Atmospheric Implications for Isoprene-Dominant Forests. *Atmos. Chem. Phys.* **2015**, *15* (9), 5145–5159.

(24) Shiraiwa, M.; Li, Y.; Tsimpidi, A. P.; Karydis, V. A.; Berkemeier, T.; Pandis, S. N.; Lelieveld, J.; Koop, T.; Pöschl, U. Global Distribution of Particle Phase State in Atmospheric Secondary Organic Aerosols. *Nat. Commun.* **2017**, *8*, 1–7.

(25) Marsh, A.; Rovelli, G.; Song, Y.-C.; Pereira, K. L.; Willoughby, R. E.; Bzdek, B. R.; Hamilton, J. F.; Orr-Ewing, A. J.; Topping, D. O.; Reid, J. P. Accurate Representations of the Physicochemical Properties of Atmospheric Aerosols: When Are Laboratory Measurements of Value? *Faraday Discuss.* **2017**, *200*, 639.

(26) Song, Y. C.; Haddrell, A. E.; Bzdek, B. R.; Reid, J. P.; Bannan, T.; Topping, D. O.; Percival, C. J.; Cai, C. Measurements and Predictions of Binary Component Aerosol Particle Viscosity. *J. Phys. Chem. A* **2016**, *120*, 8123–8137.

(27) Bzdek, B. R.; Collard, L.; Sprittles, J. E.; Hudson, A. J.; Reid, J. P. Dynamic Measurements and Simulations of Airborne Picolitre-Droplet Coalescence in Holographic Optical Tweezers. *J. Chem. Phys.* **2016**, *145* (5), 054502.

(28) Power, R. M.; Simpson, S. H.; Reid, J. P.; Hudson, A. J. The Transition from Liquid to Solid-like Behaviour in Ultrahigh Viscosity Aerosol Particles. *Chem. Sci.* **2013**, *4*, 2597–2604.

(29) Grayson, J. W.; Song, M.; Evoy, E.; Upshur, M. A.; Ebrahimi, M.; Geiger, F. M.; Thomson, R. J.; Bertram, A. K. The Effect of Adding Hydroxyl Functional Groups and Increasing Molar Mass on the Viscosity of Organics Relevant to Secondary Organic Aerosols. *Atmos. Chem. Phys.* **2017**, *17*, 8509–8524.

(30) Grayson, J. W.; Song, M.; Sellier, M.; Bertram, A. K. Validation of the Poke-Flow Technique Combined with Simulations of Fluid Flow for Determining Viscosities in Samples with Small Volumes and High Viscosities. *Atmos. Meas. Tech.* **2015**, *8* (6), 2463–2472.

(31) Marsh, A.; Petters, S. S.; Rothfuss, N. E.; Rovelli, G.; Song, Y. C.; Reid, J. P.; Petters, M. D. Amorphous Phase State Diagrams and Viscosity of Ternary Organic/Organic and Inorganic/Organic Mixtures. *Phys. Chem. Chem. Phys.* **2018**, *20*, 15086–15097.

(32) Rothfuss, N. E.; Petters, M. D. Coalescence-Based Assessment of Aerosol Phase State Using Dimers Prepared through a Dual-Differential Mobility Analyzer Technique. *Aerosol Sci. Technol.* **2016**, *50(12)*, 1294–1305.

(33) Rothfuss, N. E.; Petters, M. D. Characterization of the Temperature and Humidity-Dependent Phase Diagram of Amorphous Nanoscale Organic Aerosols. *Phys. Chem. Chem. Phys.* **2017**, *19* (9), 6532–6545.

(34) Zobrist, B.; Marcolli, C.; Pedernera, D. A.; Koop, T. Do Atmospheric Aerosols Form Glasses? *Atmos. Chem. Phys. Discuss.* **2008**, *8* (3), 9263–9321.

(35) Marshall, F. H.; Miles, R. E. H.; Song, Y.-C.; Ohm, P. B.; Power, R. M.; Reid, J. P.; Dutcher, C. S. Diffusion and Reactivity in Ultraviscous Aerosol and the Correlation with Particle Viscosity. *Chem. Sci.* **2016**, *7* (2), 1298–1308.

(36) Bosse, D. Diffusion, Viscosity, and Thermodynamics in Liquid Systems. Technical University of Kaiserslautern, Germany. *PhD Thesis* **2005**.

(37) Preston, T. C.; Reid, J. P. Accurate and Efficient Determination

of the Radius, Refractive Index, and Dispersion of Weakly Absorbing Spherical Particle Using Whispering Gallery Modes. *J. Opt. Soc. Am. B* **2013**, *30* (8), 2113.

(38) Preston, T. C.; Reid, J. P. Determining the Size and Refractive Index of Microspheres Using the Mode Assignments from Mie Resonances. *J. Opt. Soc. Am. A* **2015**, *32* (11), 2210.

(39) Cai, C.; Miles, R. E. H.; Cotterell, M. I.; Marsh, A.; Rovelli, G.; Rickards, A. M. J.; Zhang, Y.-H.; Reid, J. P. Comparison of Methods for Predicting the Compositional Dependence of the Density and Refractive Index of Organic-Aqueous Aerosols. *J. Phys. Chem. A* **2016**, *120* (33), 6604–6617.

(40) Renbaum-Wolff, L.; Grayson, J. W.; Bateman, A. P.; Kuwata, M.; Sellier, M.; Murray, B. J.; Shilling, J. E.; Martin, S. T.; Bertram, A. K. Viscosity of α-Pinene Secondary Organic Material and Implications for Particle Growth and Reactivity. *Proc. Natl. Acad. Sci. U. S. A.* **2013**, *110* (20), 8014–8019.

(41) Zhang, Y.; Sanchez, M. S.; Douet, C.; Wang, Y.; Bateman, A. P.; Gong, Z.; Kuwata, M.; Renbaum-Wolff, L.; Sato, B. B.; Liu, P. F.; et al. Changing Shapes and Implied Viscosities of Suspended Submicron Particles. *Atmos. Chem. Phys.* **2015**, *15* (14), 7819–7829.

(42) Gordon, M.; Taylor, J. S. Ideal Copolymers and the Second-Order Transitions of Synthetic Rubbers. i. Non-Crystalline Copolymers. *J. Appl. Chem.* **2007**, *2* (9), 493–500.

(43) Saleki-Gerhardt, A.; Zografi, G. Non-Isothermal and Isothermal Crystallization of Sucrose from the Amorphous State. *Pharm. Res.* **1994**, *11* (8), 1166–1173.

(44) Gallo, P.; Amann-Winkel, K.; Angell, C. A.; Anisimov, M. A.; Caupin, F.; Chakravarty, C.; Lascaris, E.; Loerting, T.; Panagiotopoulos, A. Z.; Russo, J.; et al. Water: A Tale of Two Liquids. *Chem. Rev.* **2016**, *116* (13), 7463–7500.

(45) Baldelli, A.; Power, R. M.; Miles, R. E. H.; Reid, J. P.; Vehring, R. Effect of Crystallization Kinetics on the Properties of Spray Dried Microparticles. *Aerosol Sci. Technol.* **2016**, *50* (7), 693–704.

(46) Stokes, R. H.; Robinson, R. A. Interactions in Aqueous Nonelectrolyte Solutions. I. Solute-Solvent Equilibria. *J. Phys. Chem.* **1966**, *70* (7), 2126–2131.

(47) Arrhenius, S. The Viscosity of Aqueous Mixtures. *Z. Phys. Chem.* **1887**, *1*, 285–298.

Insert Table of Contents artwork here